OPERATOR CONTROL STRATEGY IN VIRTUAL REALITY CRANE TRAINING

M. Cenkner[*], *N. Tylová*[*], *U. Michel-Schneider*[†], *P. Bouchner*[*]

Abstract: Performance assessment in simulator-based crane training commonly relies on task completion, task duration, and errors such as collisions. These measures describe task outcomes but provide limited insight into the operator's control strategy. Coordinated use of both hands and simultaneous control of multiple crane functions are widely recognized as key challenges in crane operator training. This study investigates whether interaction-based metrics derived directly from joystick signals can describe bimanual joystick control and multi-axis coordination during virtual reality mobile crane operation. Principal component analysis was used to identify the main patterns of variability in these metrics and to explore differences in control patterns across ten operators and their task executions. The observed distribution in the PCA space indicated differences among operators in the combined patterns of individual axis activation and simultaneous control of multiple crane functions.

Key words: *operator training, mobile crane, virtual reality, bimanual joystick control, principal component analysis*

Received: January 20, 2026 **DOI:** 10.14311/NNW.2026.36.002
Revised and accepted: February 27, 2026

1. Introduction

Simulation-based training has become increasingly adopted in operator training due to its ability to provide safe, repeatable, and controlled training environments. Unlike real-world training, simulation environments allow the same training scenario to be repeatedly executed under controlled conditions, enabling trainees to practice specific tasks multiple times while instructors provide immediate feedback. At the same time, other participants can observe the task execution and learn from the instructor's feedback.

Despite these advantages, evaluation practices in simulator-based operator training still tend to emphasize task completion, task duration, and the occurrence of

[*]Michal Cenkner, Petr Bouchner, Naďa Tylová – Corresponding author; Czech Technical University in Prague, Faculty of Transportation Sciences, Konviktská 20, CZ-110 00 Prague 1, Czech Republic, E-mail: tylovnad@fd.cvut.cz

[†]Ulrike Michel-Schneider; Czech Technical University in Prague, Faculty of Civil Engineering, Thákurova 7, CZ-166 29 Prague 6, Czech Republic, E-mail: ulrike.michel-schneider@fsv.cvut.cz

©CTU FTS 2026

errors or collisions. In practice, these indicators are often complemented by instructor observation, which is valuable for training but difficult to standardize or compare across trainees. Although these measures are useful for evaluating task execution, they provide limited insight into how operators coordinate control inputs during task execution.

In crane operation, coordinated bimanual control has been identified by instructors as an important aspect of operator training. Operators are required to simultaneously manipulate multiple functions using two joysticks, where each joystick axis controls a different movement of the crane system. The analysis investigates whether operators differ in the relative combination of metrics describing individual axis activation and the simultaneous control of multiple crane functions. Accordingly, this study is focused on two objectives:

- Objective 1: To derive interaction-based metrics characterizing individual axis activation and the simultaneous control of multiple crane functions during VR crane operation.
- Objective 2: To explore whether operators differ in the relative combination of these metrics across task executions.

2. State of the Art

2.1 Simulator-Based Operator Training

Simulator-based training is widely used in domains where practice on real equipment is constrained by safety risks, high operating costs, limited machine availability, or the need to avoid disruption of normal operations [1, 2]. A simulator enables trainees to repeat the same task under controlled conditions and allows instructors to introduce hazardous, rare, or technically demanding situations without exposing personnel or equipment to real consequences [3]. These properties are particularly relevant to heavy-machinery operation, where practical training requires large workspaces, expensive equipment, and close supervision. Studies involving mobile equipment, including forestry machines, have therefore examined simulators not only as introductory training tools, but also as environments in which operators can practise control procedures before working with real machinery [4–6].

Virtual reality extends conventional simulation by placing the trainee inside an interactive three-dimensional representation of the working environment. This can support spatial understanding, visual scanning, and recognition of relationships among the machine, transported objects, obstacles, and target areas [7, 8]. Such capabilities are relevant to construction and crane operation, where safe task execution depends on continuous perception of the surrounding workspace. Immersive head-mounted displays can increase presence and perceived realism, and their use has been investigated in both construction-equipment safety training and crane-operator training [9, 10]. However, immersion alone does not guarantee effective learning. The suitability of VR depends on the training objective, the realism of the simulated task and controls, and the correspondence between actions performed in the simulator and those required on the real machine [2, 11]. Reported limitations include visual discomfort, cybersickness, technical restrictions, and the risk that an

insufficiently realistic interface may train behaviours that do not transfer directly to real operation [2, 11].

Besides providing a safe training environment, simulators offer an important methodological advantage: operator behaviour and system responses can be recorded automatically and under repeatable conditions. Depending on the simulation, recorded data may include task events, completion times, errors, trajectories, machine states, and control inputs [3, 12, 13]. This makes it possible to compare operators, tasks, or repeated training sessions without relying exclusively on instructor observation. Simulator data have consequently been used to examine training effectiveness, skill development, and differences in operating behaviour across a range of industrial and heavy-equipment applications [5, 12, 14]. The simulator can therefore be regarded not only as a training device, but also as a standardized experimental platform for operator assessment. This distinction is important because the information available from the simulator may describe both the outcome of a task and the process by which the operator achieved it.

2.2 Operator Assessment in Simulator-Based Training

Operator assessment in simulator-based training can combine instructor observation, subjective questionnaires, and objective performance measures. Instructor feedback remains important for identifying errors and guiding further practice, although its content may depend on the experience and judgement of the evaluator [14]. Questionnaires provide complementary information about how the trainee perceives the task and the training system. They may address workload, confidence, usability, presence, or perceived usefulness [4, 6, 10]. Objective assessment, in contrast, commonly relies on indicators such as task completion, completion time, positioning accuracy, collisions, errors, or simulator scores [5, 12, 13]. These indicators allow consistent comparison across operators and training sessions, but they primarily describe the result of task execution rather than the control process itself.

To examine how the task was performed, several studies have analysed behavioural and system data recorded during equipment operation. Such process-related measures include joystick or lever activity, trajectories, movement smoothness, control-input segments, and the simultaneous use of multiple machine functions. Dreger et al. evaluated the development of bimanual control using the number of joystick input segments [15]. Polowy and Rutkowski included the number of simultaneously controlled crane functions when analysing the learning curves of harvester operators [12]. Sekizuka et al. derived indicators from excavator lever operation and bucket movement to distinguish different levels of operator skill [13]. Other studies have combined control data with visual behaviour; for example, Koskinen and Bednarik compared expert and novice forest-machine operators through the relationship between gaze and boom movement [16]. These approaches show that recorded interaction data can reveal differences in operating behaviour that are not visible from task outcomes alone.

This distinction is particularly important in crane operation, where several machine functions are controlled through two hands and multiple joystick axes. Research on bimanual motor learning indicates that skill acquisition involves changes

in coordination, movement organisation, and the stability of control strategies, in addition to improvements in task performance [17–19]. Existing studies have examined individual control inputs, input segments, or the number of simultaneously used functions. However, these measures do not fully describe which hands and joystick axes are combined during task execution. Less attention has therefore been given to recurring patterns of coordinated dual-hand control and to differences in these patterns among operators and tasks. The present study addresses this gap by deriving interaction-based metrics that describe individual axis activity, simultaneous use of both axes of one joystick, and coordinated control involving both hands. These metrics are intended to complement conventional outcome measures and subjective assessment by providing an objective description of operator control strategy.

3. Experimental Framework

3.1 Testing Environment

The experimental framework was designed using a virtual reality mobile crane simulator. The simulator combines a physical operator workstation with an immersive virtual environment, allowing participants to operate the crane via a control interface consistent with a real mobile crane. During each experimental session, operator interaction with the virtual environment was continuously recorded for subsequent analysis.

The hardware part of the simulator consists of a physical operator seat, armrests equipped with joysticks, and a simplified cabin frame (Fig. 1, left). The simulator platform is complemented by a Meta Quest 3 virtual-reality headset, which provides the visual scene from the operator's perspective (Fig. 1, right). This combination enables the operator to interact with the virtual crane environment using physical controls corresponding to those of a real machine.



Fig. 1 *Simulator setup and operator view. The left view shows the physical simulator platform with the operator seat, control interfaces, simulation computer, and VR headset. The right view shows the virtual crane cabin and interactive scene from the operator's perspective.*

The virtual environment was implemented in the Unity engine. The scene represents a construction site located on the outskirts of a municipality and was prepared to cover a wide vertical and horizontal working range around the crane. The workspace contains an underground level, a ground level, a vehicle loading level, a mid-rise building level, and a high-rise building level. Loads are transferred between predefined pick-up and drop-off zones distributed around the crane within a 360° operating area. Their distance from the cabin and their height level vary between tasks, which creates different demands on spatial orientation and coordinated joystick control.

Only the transported loads and the target zones were interactive. The surrounding construction environment acts as a static reference scene, while collision detection is implemented for contacts between the crane, the load, and obstacles. When a collision occurs, the simulator provides visual and acoustic feedback. This makes it possible to keep the training task safe and repeatable, while still preserving operational constraints that are relevant for crane handling. Fig. 2 illustrates the layout of the interactive scene used in the crane experiment. The left view shows the spatial arrangement of the loads from above, while the right view presents the height levels of the pick-up and drop-off zones.

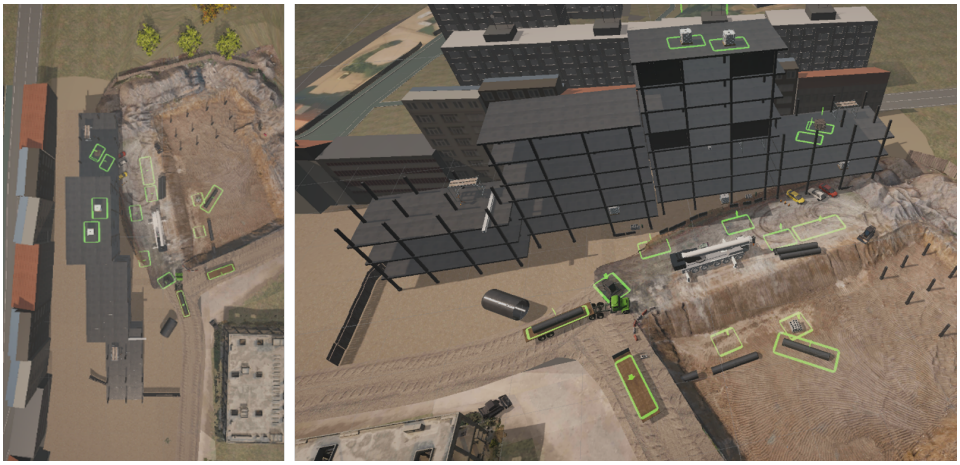


Fig. 2 *Virtual construction-site scene used in the experiment, with task-related load positions and interaction zones highlighted in green.*

3.2 Experimental Procedure

The experimental scenario was structured as a sequence of 10 load-transfer tasks. Before the session, each participant was given time to become familiar with the simulator environment, the joystick controls, and the task interface. Initially, only the overall structure of the scenario was explained. The exact configuration and order of the individual tasks were not disclosed, requiring participants to rely on their own control strategy. Each task followed the same interaction sequence. The task started with the visual indication of the target load. Once the load had been

picked up, the corresponding drop-off zone was highlighted. Placing the load in the designated drop-off zone automatically completed the current task and indicated the next load.

The parameters of all tasks are summarized in Tab. I. Positive and negative rotation angles indicate clockwise and counterclockwise cabin rotation, respectively. The notation $+45 \rightarrow -90$ indicates that the operator first rotates the cabin 45° clockwise toward the load and, after picking up the load, rotates the cabin 90° counterclockwise toward the drop-off location. The height notation (L1–L5) describes the initial position of the crane hook, the pick-up location, and the final drop-off location of the load. For example, the sequence L2 → L1 → L4 indicates that the crane hook is initially positioned at height level L2, picks up the load at L1, and places it at L4.

Task	Description	Rotation (°)	Height level
1	Take the load from the underground level and place it on the top of the mid-rise building.	$+45 \rightarrow -90$	L2→L1→L4
2	Take the load from the top of the mid-rise building and place it at the underground level.	$0 \rightarrow +135$	L4→L4→L1
3	Take the load from the underground level and place it on the vehicle.	$-45 \rightarrow +90$	L1→L1→L3
4	Take the load from the vehicle and place it at ground level.	$+45 \rightarrow -180$	L3→L3→L2
5	Take the load from the high-rise building and place it at ground level.	$-90 \rightarrow +45$	L2→L5→L2
6	Take the load from the ground level and place it on the vehicle.	$+45 \rightarrow +180$	L2→L2→L3
7	Take the load from the high-rise building and place it at ground level.	$+90 \rightarrow -45$	L3→L5→L2
8	Take the load from the area next to the vehicle and place it on the top of the mid-rise building.	$-45 \rightarrow -225$	L2→L2→L4
9	Take the load from the mid-rise building and place it at the underground level.	$0 \rightarrow +90$	L4→L4→L1
10	Take the load from the vehicle and place it at ground level.	$+45 \rightarrow -90$	L1→L1→L2

Tab. I *List of the ten crane-operation tasks, including the cabin rotations toward the pick-up and drop-off positions and the height levels of the initial hook position, the load, and the drop-off zone.*

3.3 Data Acquisition and Processing

The final dataset included 10 male operators. The participants represented a range of technical professions related to crane operation, maintenance, and training. Their ages ranged from 24 to 61 years (mean = 41.6 years, SD = 11.4 years). Before the experimental session, the operators subjectively classified their level of previous crane-operation experience in consultation with the experiment supervisor. The novice level included Operators 2, 3, 4, and 9; the intermediate level included Operators 1 and 7; and the experienced level included Operators 5, 6, 8, and 10.

The four joystick axes were recorded at a sampling frequency of 30 Hz as input values in the range from −1 to 1, where 0 represents the neutral joystick position. The corresponding crane functions controlled by each joystick axis are summarized in Tab. II. In addition to the joystick input signals, the recorded data included crane state variables together with task identifiers and timestamps corresponding to task start, load pick-up, and load placement. These event markers were subsequently used to segment the continuous recording into individual task executions.

Prior to the analysis, missing joystick samples were replaced by the neutral joystick position, the signals were smoothed using a median filter with a window size of three samples, and a joystick-specific dead-zone was applied to suppress small involuntary control inputs around the neutral position. The dead-zone intervals were determined by comparing each joystick input signal with the corresponding crane response. Input ranges within which changes in the joystick signal produced no change in the corresponding response were treated as dead zones.

Label	Joystick axis	Crane function	Dead-zone interval
LX	Left side	Cabin rotation	[−0.20, 0.30]
LY	Left forward	Boom extension	[−0.31, 0.15]
RX	Right side	Boom lifting	[−0.30, 0.05]
RY	Right forward	Rope length	[−0.05, 0.05]

Tab. II *Joystick axis labels, associated crane functions, and dead-zone intervals applied to the recorded joystick input signals.*

3.4 Data Analysis

The proposed interaction-based metrics were designed to characterize patterns of joystick use and coordination rather than general task-completion performance. Their definition was motivated by discussions with experienced crane operators and training specialists during the preparation of the experimental framework, which identified coordinated bimanual control as one of the key skills developed during crane operator training. The proposed interaction-based metrics are summarized in Tab. III.

The proposed interaction-based metrics are grouped according to the type of joystick activity they describe. The first group quantifies the activity of individual joystick axes, the second group describes simultaneous dual-axis control of a single

joystick, and the remaining metrics characterize coordinated dual-hand control. The single-axis and dual-axis metrics are not mutually exclusive because simultaneous dual-axis operation inherently includes the activity of both individual axes.

In contrast, the dual-hand metrics (DHS, DHC, DHT, and DHD) are defined as mutually exclusive coordination states, ensuring that each sample involving both hands is assigned to exactly one category according to the number and combination of active joystick axes. This exclusive definition enables a consistent quantification of different levels of bimanual coordination while preventing multiple assignments of the same control action.

Metric	Active joystick axes	Description
LX, LY	LX, LY	Activity of an individual joystick axis.
RX, RY	RX, RY	
SHDL	LX + LY	Simultaneous control of both axes of one joystick.
SHDR	RX + RY	
DHS	LX + RX or LY + RY	Simultaneous use of both hands, controlling the same/opposite axes.
DHC	LX + RY or LY + RX	
DHT	LX + LY + RX/RY RX + RY + LX/LY	Simultaneous use of both hands with exactly three active joystick axes.
DHD	LX + LY + RX + RY	Simultaneous use of both hands with all four joystick axes active.

Tab. III *Interaction-based metrics used to characterize patterns of joystick use and coordination, including the corresponding joystick-axis combinations and descriptions.*

The recorded time-series data were segmented into individual tasks using the predefined event markers stored in the measurement logs. Each task was identified by three consecutive events: START, PICKUP, and DROP. The interval between START and DROP was considered a single task execution and treated as an individual observation for subsequent analysis. Since the experimental scenario was designed as a continuous sequence of tasks, each DROP event was immediately followed by the START event of the next task.

For each task, the occurrence of every interaction metric was quantified as the relative proportion of samples in which the corresponding activity state was present. Let $S_i(t)$ denote the binary activity state associated with interaction metric i, where $S_i(t) = 1$ if the activity state is present at sample t, and $S_i(t) = 0$ otherwise. The value of each interaction metric was then computed as

$$M_i = \frac{1}{N} \sum_{t=1}^{N} S_i(t), \tag{1}$$

where M_i denotes the value of the ith interaction metric ($i = 1, \ldots, 10$), N is the total number of samples within the segmented task, and $S_i(t)$ is the binary activity state corresponding to interaction metric i, as defined in Tab. III. Consequently,

each interaction metric represents the relative proportion of task duration during which the corresponding interaction state was observed.

Each segmented task was treated as an individual behavioral observation and represented by a ten-dimensional feature vector containing the interaction metrics computed from the joystick activity states of the corresponding task,

$$\mathbf{x}_j = [M_{ji}]_{i=1}^{10}, \qquad \mathbf{x}_j \in \mathbb{R}^{1\times 10}, \tag{2}$$

where M_{ji} denotes the value of the ith interaction metric for the jth task observation. The feature vectors corresponding to all task observations were subsequently assembled into the feature matrix

$$\mathbf{X} = \begin{bmatrix} \mathbf{x}_1 \\ \mathbf{x}_2 \\ \vdots \\ \mathbf{x}_J \end{bmatrix}, \qquad \mathbf{X} \in \mathbb{R}^{J\times 10}, \tag{3}$$

where J denotes the total number of behavioral observations. Given the limited dataset and the exploratory nature of the study, each of the ten distinct tasks performed by each operator was treated as a separate observation, allowing task-related variability to be represented in the analysis. The resulting feature matrix consisted of 100 rows (10 operators $\times$ 10 tasks) and 10 columns corresponding to the proposed interaction metrics.

Prior to principal component analysis (PCA), the feature matrix $\mathbf{X}$ was standardized using z-score normalization to obtain zero mean and unit variance for each interaction metric, thereby eliminating scale differences and ensuring comparable contribution of all variables to the analysis. The standardized feature values were computed as

$$z_{ji} = \frac{x_{ji} - \mu_i}{\sigma_i}, \tag{4}$$

where x_{ji} denotes the value of the ith interaction metric for the jth task observation, while μ_i and σ_i represent the mean value and standard deviation of the ith interaction metric computed across all task observations. The standardized observations were subsequently arranged into the feature matrix

$$\mathbf{Z} = \begin{bmatrix} \mathbf{z}_1 \\ \mathbf{z}_2 \\ \vdots \\ \mathbf{z}_J \end{bmatrix}, \qquad \mathbf{Z} \in \mathbb{R}^{J\times 10}, \tag{5}$$

where J denotes the total number of task observations. The next step consisted of computing the covariance matrix to quantify relationships and patterns of joint variability among the extracted interaction metrics. The covariance matrix was computed as

$$\mathbf{C} = \frac{1}{J-1}\mathbf{Z}^{\mathrm{T}}\mathbf{Z}, \tag{6}$$

where $\mathbf{C} \in \mathbb{R}^{10\times10}$ denotes the covariance matrix. Principal directions of variability were subsequently determined by solving the eigenvalue problem

$$\mathbf{C}\mathbf{v} = \lambda\mathbf{v}, \tag{7}$$

where $\mathbf{v}$ denotes an eigenvector and λ the corresponding eigenvalue. The eigenvectors were subsequently sorted in descending order according to their corresponding eigenvalues, such that the principal components explaining the largest proportion of variance were placed first. The eigenvectors were arranged into the loading matrix

$$\mathbf{W} = [\mathbf{v}_1, \mathbf{v}_2, \ldots, \mathbf{v}_{10}], \qquad \mathbf{W} \in \mathbb{R}^{10\times10}, \tag{8}$$

The standardized feature matrix was subsequently projected onto the principal component space according to

$$\mathbf{Y} = \mathbf{Z}\mathbf{W}, \tag{9}$$

where $\mathbf{Y} \in \mathbb{R}^{J\times10}$ contains principal component scores for all task observations. The PCA was implemented in MATLAB using the built-in pca() function, which returned three principal outputs: *coeff*, *score*, and *latent*, corresponding to the loading matrix $\mathbf{W}$, the principal component scores $\mathbf{Y}$, and the eigenvalues λ, respectively.

Task duration was not included as an additional interaction metric or as an input variable in the PCA because the analysis focused on the relative use of joystick control strategies rather than on general task-completion performance or operator ranking. Nevertheless, task duration already affects the proposed interaction metrics through their normalization by the total number of samples in each task execution: a prolonged period of inactivity would increase the task duration and consequently reduce the relative activation of the corresponding control states. Absolute task duration was therefore reviewed separately as a data-quality indicator to identify unusually long executions and to verify, through inspection of the corresponding joystick time series, whether they contained prolonged inactivity or recording errors that could distort the interaction metrics.

4. Results

This section focuses on interaction metrics derived from joystick activity, with each task execution represented by the relative occurrence of single-axis activity, within-hand dual-axis control, and coordinated bimanual control. Principal component analysis was used to identify the main patterns of variability in these metrics and to describe differences in operator control strategies. The results include an overview of PCA loading coefficients, the distribution of operators and task executions in the PCA space, and examples of the underlying control-signal patterns for selected operators and tasks.

4.1 PCA Loadings Analysis

The PCA loading analysis focused on the first three principal components, which together accounted for 71.89 % of the total variance in the dataset. The loading coefficients describe the contribution of individual interaction metrics to each component, with higher absolute values indicating stronger contributions. The sign of the loading indicates the direction of the relationship within the PCA space. The corresponding loading coefficients and the variance explained by each component are reported in Tab. IV.

Metric	PC1	PC2	PC3
LX	−0.1593	−0.3369	0.5155
LY	0.2810	0.4921	0.1448
RX	0.3772	−0.3427	−0.0078
RY	0.3844	−0.2006	−0.2495
SHDL	0.2144	0.3554	0.5213
SHDR	0.4355	−0.3321	−0.0706
DHS	0.2574	0.2468	−0.3494
DHC	−0.1297	−0.4196	0.1951
DHT	0.4755	−0.1008	0.1385
DHD	0.2462	0.0520	0.4413
Explained variance (%)	32.85	24.09	14.95

Tab. IV *PCA loading coefficients for the ten interaction-based metrics across the first three principal components. The final row reports the variance explained by each component.*

PC1 explained 32.85 % of the total variance and was mainly defined by DHT (0.4755), SHDR (0.4355), RY (0.3844), and RX (0.3772). This indicates that the strongest source of variability was associated with right-hand activity and three-axis bimanual coordination. The opposite direction of this component was represented mainly by LX (−0.1593) and DHC (−0.1297), although their lower absolute values indicate a weaker contribution. PC2 explained 24.09 % of the variance and was characterized primarily by LY (0.4921) and DHC (−0.4196), suggesting a contrast between left-hand forward control and cross-hand coordination. PC3 explained 14.95 % of the variance and was mainly associated with SHDL (0.5213), LX (0.5155), and DHD (0.4413), indicating variability related to left-hand dual-axis control and full four-axis coordination.

4.2 PCA Score Analysis by Operator

To examine operator-specific control strategies, the mean PC1 and PC2 scores were calculated for each operator across all task executions. The mean position represents the operator's average interaction pattern in the PCA space, while the

standard deviation in both directions indicates the variability of this pattern across tasks. These operator-specific scores and their standard deviations are shown in Fig. 3. Operators 3 and 4 occupied opposite diagonal regions of the PCA space, suggesting clearly different control strategies. Operator 3 was positioned towards negative PC1 and positive PC2 values, whereas Operator 4 showed the opposite tendency, with positive PC1 and negative PC2 values. Operator 10 was located closer to the center of the PCA space, but showed one of the largest standard deviations, suggesting that this operator adapted the control strategy more strongly to the characteristics of individual tasks.

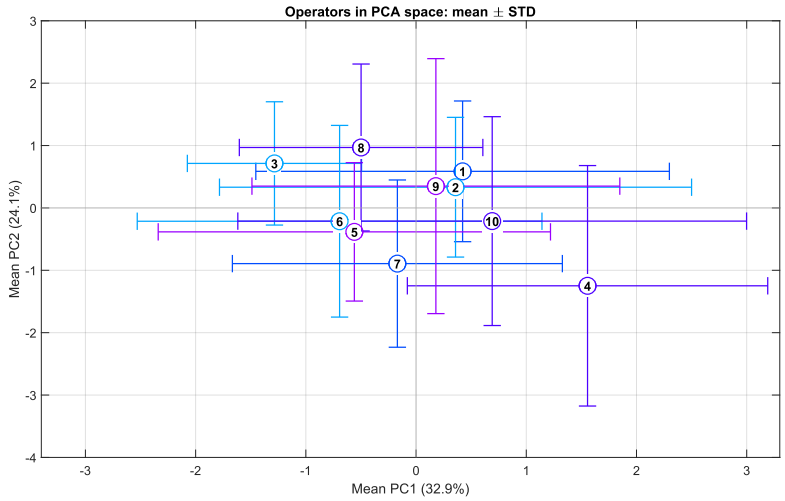


Fig. 3 *Mean PC1 and PC2 scores for individual operators across all task executions. Horizontal and vertical error bars indicate the corresponding standard deviations.*

The interpretation of the operator score distribution was further supported by the z-score heatmap of mean interaction metrics for individual operators shown in Fig. 4. The values indicate whether each operator used a given interaction metric more or less frequently than the dataset average. Operator 4 showed above-average values for RX, RY, SHDR, DHT, and DHD, together with a below-average value of LY, which is consistent with its position in the positive-PC1 and negative-PC2 region and indicates a strategy characterized by pronounced right-hand activity and coordinated multi-axis control. In contrast, Operator 3 showed below-average values across most interaction metrics, particularly RX, RY, SHDR, and DHT, consistent with its negative PC1 position. Operator 10 was located close to the center of the PCA space, and the heatmap confirmed that most of its interaction metrics remained close to the dataset average. Only SHDR and DHT showed clearly above-average values, which contributed to a slight shift towards positive PC1 and negative PC2.

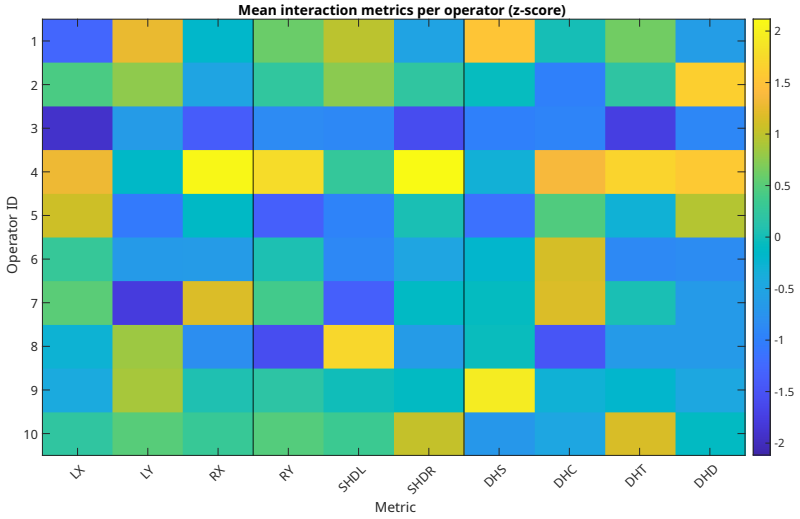


Fig. 4 *Z-score heatmap of the mean interaction-based metrics for individual operators. Positive and negative values indicate values above and below the dataset mean, respectively.*

4.3 PCA Score Analysis by Task

The PCA score distribution for individual tasks was used to compare control patterns across task executions. Fig. 5 shows the mean PC1 and PC2 scores for individual tasks. Tasks with similar demands on crane-function use, particularly

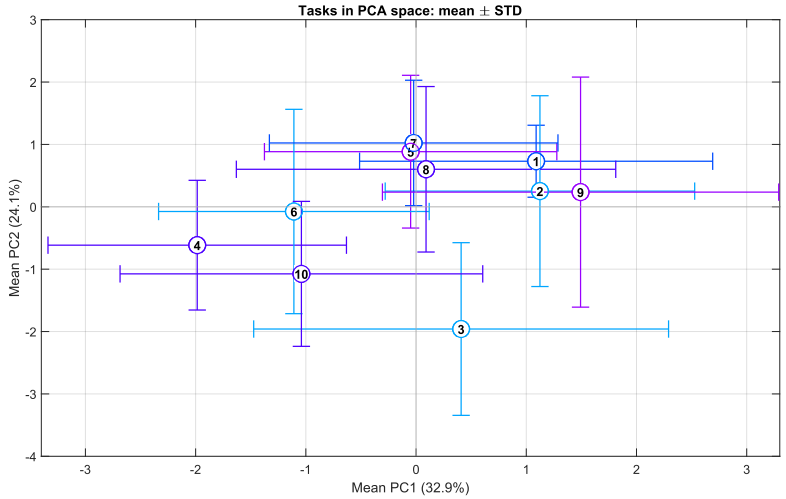


Fig. 5 *Mean PC1 and PC2 scores for individual tasks across all operators. Error bars indicate the corresponding standard deviations.*

in terms of cabin rotation and vertical movement, were located close to each other in the PCA space. Tasks 5 and 7 were located close together and both involved load manipulation on the high-rise building.

In contrast, Tasks 1, 2, and 9 formed a separate group associated with the mid-rise building. Task 8 was located between these two groups. Although its target was on the mid-rise building, the task allowed different trajectory choices: operators could either use a path with a larger cabin rotation or choose a shorter rotation path through the highest part of the working area. Since the trajectory was not prescribed, the position of Task 8 in the PCA space may reflect these alternative control patterns. Task 4 formed a distinct case, characterized mainly by cabin rotation and only a small vertical difference between the initial and final load positions. Overall, the correspondence between the predefined task characteristics and their positions in the PCA space indicates that the proposed metrics captured differences in the control demands of the scenarios and supports the suitability of the task design for representing diverse combinations of crane-function use.

The heatmap for individual tasks shown in Fig. 6 provides a direct comparison of the z-score values of interaction-based metrics across individual tasks. It shows which metrics were above or below the dataset average for each task and helps relate the PCA score distribution to specific control patterns. Task 10 showed a clearly increased value of LX, reflecting the dominant use of cabin rotation during task execution. In contrast, Task 4 showed below-average values across most interaction metrics, indicating lower relative activation of the control and coordination states represented by these metrics. Tasks 1, 2, and 9 showed similar profiles, with increased values of coordinated metrics DHT and DHD, together with higher right-hand activity represented by RX and RY. These similarities in the metric profiles correspond to the proximity of these tasks in the PCA space and show how the proposed metrics can be used to assess the control demands of individual tasks.

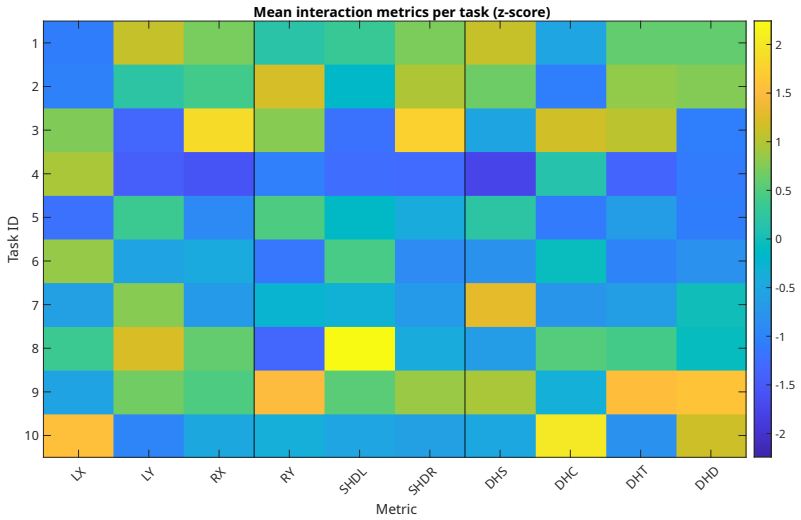


Fig. 6 *Z-score heatmap of the mean interaction-based metrics for individual tasks.*

4.4 Task Duration Overview

Task duration was examined as a complementary measure to identify unusually long executions and support the inspection of potential outliers. Fig. 7 shows the total duration of each operator–task combination together with the durations of the two task phases: from task start to load pick-up and from pick-up to drop-off.

Execution times varied across both tasks and operators. The longest total duration was observed for Operator 3 in Task 2 and was primarily associated with the start-to-pick-up phase. A longer execution was also observed for Operator 8 in Task 7, again mainly before load pick-up. The pick-up-to-drop-off phase showed lower absolute durations but noticeable variability, particularly for Tasks 1 and 8. Overall, the heatmaps indicate that longer execution times occurred in individual operator–task combinations rather than consistently across all executions of a particular task. Recordings with notably longer durations were inspected, and no prolonged inactive periods that would justify their exclusion from the analysis were identified.

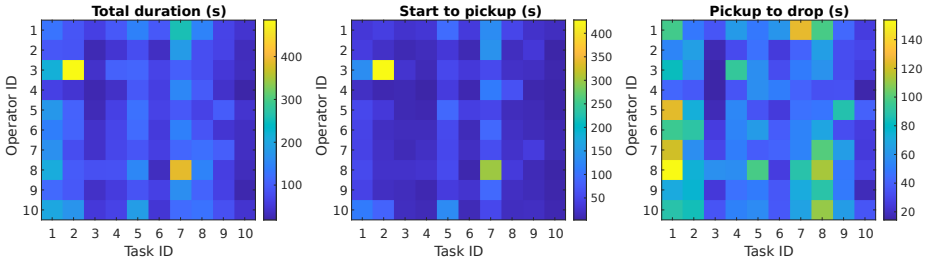


Fig. 7 *Task duration for all operator–task combinations. The panels show total task duration, duration from task start to load pick-up, and duration from pick-up to drop-off. Colors represent duration in seconds.*

4.5 Selected Operator–Task Comparison

Tasks 4 and 8 were selected as illustrative examples of different control demands. Task 4 required cabin rotation and involved only a small vertical difference between the initial and final load positions, whereas Task 8 required the load to be transferred from a position close to the crane to a mid-rise building located on the opposite side. Its execution combined substantial cabin rotation with adjustments of the boom configuration and rope length.

As shown in Fig. 8, Tasks 4 and 8 produced different distributions of operator scores in the PCA space. The scores for Task 4 were located mainly towards negative PC1 values for most operators, whereas the scores for Task 8 extended towards higher PC1 and PC2 values. As also indicated by the metric heatmap in Fig. 6, Task 4 was characterized primarily by LX and RY activation, together with the corresponding DHC coordination metric. This reflects the nature of the task, in which operators relied mainly on cabin rotation and rope-length adjustment.

In contrast, Task 8 was characterized by an above-average proportion of SHDL, indicating simultaneous cabin rotation and boom-extension adjustment. This cor-

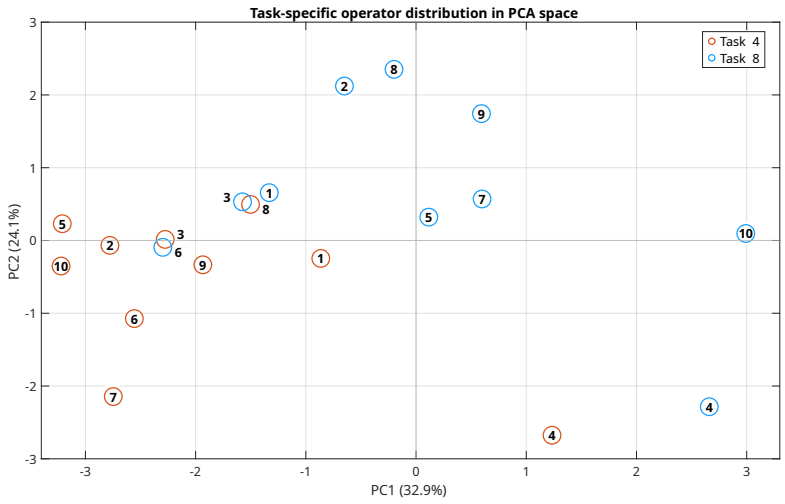


Fig. 8 *PC1–PC2 score distribution of individual operators for Tasks 4 and 8. Each labeled point represents an operator's score for the corresponding task.*

responds to the loadings in Table IV, where LY and SHDL contribute to positive PC2 scores. Right-hand activation metrics and DHT have positive PC1 and negative PC2 loadings, whereas DHD has a positive PC1 loading and only a small positive PC2 loading, placing it close to the PC1 axis. The broader distribution of Task 8 scores therefore reflects differences among operators in the particular combination and coordination of control inputs used to complete the task.

Based on their average scores in the PCA space, Operators 3, 4, and 10 were selected as illustrative examples of different control patterns and for a closer inspection of the original time-series data. Operators 3 and 4 represented contrasting control patterns in the PCA space, with Operator 3 positioned towards negative PC1 and positive PC2 values and Operator 4 showing the opposite tendency. Operator 10 was positioned closer to the centre of the PCA space, but its Task 8 score shifted markedly towards positive PC1. Their Task 8 recordings were therefore visualized to show how the differences captured by the proposed metrics appear in the original joystick inputs, normalized crane responses, task phases, task duration, and the relative occurrence of dual-hand coordination metrics.

Fig. 9 shows the original control signals (blue) and crane function responses normalized to the range $[0, 1]$ (orange) for the selected operators during Task 8. The SCENARIO markers indicate task start, load pick-up, and load drop-off. The side panel reports the duration of each phase and the total task duration. It also includes the relative occurrence of the dual-hand coordination metrics DHS, DHC, DHT, and DHD. Operator 10 showed the highest proportion of DHD (0.062) and also a high value of DHT (0.231). Operator 4 showed increased values mainly for DHC (0.127) and DHT (0.187). Operator 3 had the highest value of DHC (0.207), while the remaining coordinated metrics were low compared with the other displayed operators.

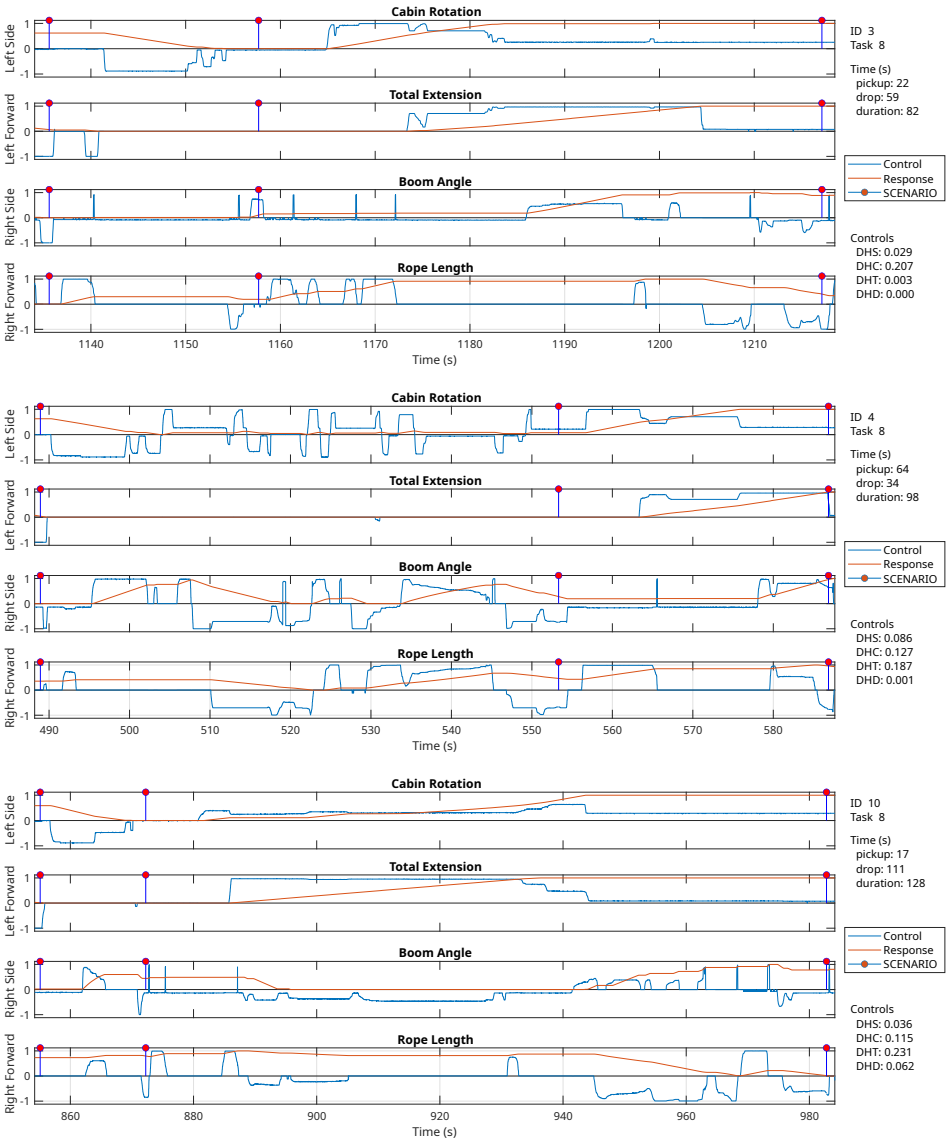


Fig. 9 *Control inputs and normalized crane responses for selected operators during Task 8. The blue curves represent joystick control signals, the orange curves represent normalized crane responses, and the markers indicate scenario events.*

5. Discussion

The results show that joystick-derived interaction metrics can provide a structured description of bimanual control patterns during VR crane operation. In this context, PCA scores were used to compare similarities between operators and task executions, while loading coefficients helped identify which interaction-based metrics contributed most strongly to the observed variability. The main contribution of the study is therefore the demonstration that the relative use and coordination of joystick axes can provide additional information about operator control patterns beyond the inspection of raw control signals or conventional task-performance measures alone.

Task duration was used to contextualize the time-series recordings and identify atypical task executions for further inspection as potential outliers. Although shorter completion times may indicate more fluent execution, they do not explain how the operator used and coordinated the controls. Task duration was also used to normalize the interaction metrics, which represented the relative occurrence of individual joystick activation and coordination states. Consequently, inactive periods and sequential rather than simultaneous inputs could affect the distribution of these metrics.

Operators assigned to the same experience level were expected to exhibit similar control patterns. However, no consistent similarities corresponding to the predefined experience levels could be identified in the dataset. This may partly reflect the subjective classification of operator experience, together with the small and unbalanced groups. The analysis focused on observable differences between individual operators rather than on validating an expert–novice classification. The observed control patterns therefore cannot be interpreted as more or less appropriate without a task-specific expected strategy defined by the trainer or scenario designer.

The immersive nature of VR provides a suitable environment for practising bimanual control and coordination. However, simulator-induced motion sickness may limit its suitability for some participants, while limited physical fidelity restricts the transferability of findings to real crane operation. Previous experience with VR systems was not systematically recorded and could therefore not be considered when interpreting differences between operators. The proposed assessment is therefore intended primarily to support bimanual control training; proficiency in the simulator does not demonstrate competence in operating a real crane, although acquired sensorimotor familiarity may facilitate subsequent adaptation.

Future work should validate the proposed metrics using a larger and more balanced dataset, with operator experience levels defined according to objective and reproducible criteria. Trainer assessments could help determine how the identified control patterns relate to task execution quality and support the definition of task-specific expected strategies. Repeated measurements could further show whether the interaction metrics capture changes in control strategy during training and contribute to more targeted feedback.

6. Conclusion

This study investigated whether joystick-derived interaction metrics can be used to describe bimanual control during VR crane operation. The proposed metrics quantified the relative use of individual joystick axes, simultaneous control within each hand, and coordinated control across both hands. PCA showed differences in the relative representation of these metrics across individual task executions. However, no consistent control strategies corresponding to task types or predefined operator experience levels could be identified.

The results demonstrate that interaction-based metrics provide information about how operators use and coordinate joystick inputs that is not captured by task completion time alone. Their interpretation nevertheless requires a task-specific expected strategy and validation against conventional performance measures and trainer assessments. Future studies using larger and more balanced samples and repeated measurements should determine whether these metrics can capture changes in bimanual control during training and contribute to more targeted simulator-based feedback.

Acknowledgement

This study was supported by the Technology Agency of the Czech Republic (TAČR) – program TREND under the project Cabin Simulator for Anthropometric Research and Operator Training FW10010376). The authors would also like to thank TADANO and 1to1design for organizing the workshop and supporting the experimental measurements.

References

[1] BURK E., HAN H.-S., SMIDT M.F., FOX B. Incorporating Simulators into a Training Curriculum for Forestry Equipment Operators: A Literature Review. *Croatian Journal of Forest Engineering*. 2024, 45(1), pp. 199–215, doi: 10.5552/crojfe.2024.2142.

[2] STEFAN H., MORTIMER M., HORAN B. Evaluating the effectiveness of virtual reality for safety-relevant training: a systematic review. *Virtual Reality*. 2023, 27, pp. 2839–2869, doi: 10.1007/s10055-023-00843-7.

[3] PATLE D.S., MANCA D., NAZIR S., SHARMA S. Operator training simulators in virtual reality environment for process operators: a review. *Virtual Reality*. 2019, 23, pp. 293–311, doi: 10.1007/s10055-018-0354-3.

[4] BURK E., HAN H.-S., SMIDT M., FOX B. Effectiveness of simulator training compared to machine training for equipment operators in the logging industry. *International Journal of Forest Engineering*. 2023, 34(3), pp. 373–384, doi: 10.1080/14942119.2023.2194751.

[5] LEE E., MUN H., LIM H., PARK S. The Efficacy of Simulator Technology for Forwarder Operator Training: A Preliminary Study in South Korea. *Forests*. 2025, 16(6), pp. 882, doi: 10.3390/f16060882.

[6] SOLOVEY E.T., ZEC M., PFEUFFER K., MÜHL C. Cognitive workload assessment during VR forklift training. *International Journal of Industrial Ergonomics*. 2025, 51, pp. 79–89, doi: 10.1016/j.ergon.2025.103718.

[7] LI X., YI W., CHI H.-L., WANG X., CHAN A.P.C. A critical review of virtual and augmented reality (VR/AR) applications in construction safety. *Automation in Construction*. 2018, 86, pp. 150–162, doi: 10.1016/j.autcon.2017.11.003.

[8] WANG P., WU P., WANG J., CHI H.-L., WANG X. A Critical Review of the Use of Virtual Reality in Construction Engineering Education and Training. *International Journal of Environmental Research and Public Health*. 2018, 15(6), pp. 1204, doi: 10.3390/ijerph15061204.

[9] SHRINGI A., ARASHPOUR M., GOLAFSHANI E.M., RAJABIFARD A., DWYER T., LI H. Efficiency of VR-Based Safety Training for Construction Equipment: Hazard Recognition in Heavy Machinery Operations. *Buildings*. 2022, 12(12), pp. 2084, doi: 10.3390/buildings12122084.

[10] SONG H., KIM T., KIM J., AHN D., KANG Y. Effectiveness of VR crane training with head-mounted display: Double mediation of presence and perceived usefulness. *Automation in Construction*. 2021, 122, pp. 103506, doi: 10.1016/j.autcon.2020.103506.

[11] JENSEN L., KONRADSEN F. A review of the use of virtual reality head-mounted displays in education and training. *Education and Information Technologies*. 2018, 23(4), pp. 1515–1529, doi: 10.1007/s10639-017-9676-0.

[12] POLOWY K., RUTKOWSKI D. Learning Curves of Harvester Operators in a Simulator Environment. *Forests*. 2024, 15(8), pp. 1277, doi: 10.3390/f15081277.

[13] SEKIZUKA R., ITO M., SAIKI S., YAMAZAKI Y., KURITA Y. System to Evaluate the Skill of Operating Hydraulic Excavators Using a Remote Controlled Excavator and Virtual Reality. *Frontiers in Robotics and AI*. 2020, 6, pp. 142, doi: 10.3389/frobt.2019.00142.

[14] MARCANO L., HAUGEN F.A., SANNERUD R., KOMULAINEN T. Review of simulator training practices for industrial operators: How can individual simulator training be enabled?. *Safety Science*. 2019, 115, pp. 414–424, doi: 10.1016/j.ssci.2019.02.019.

[15] DREGER F. A., CHUANG L.L., RINKENAUER G. Analysis of learning the bimanual control of (tele)operating joint space controlled robotic arms with 4 degrees of freedom using the two-timescales power law of learning. *Ergonomics*. 2024, 67(6), pp. 759–771, doi: 10.1080/00140139.2023.2270784.

[16] KOSKINEN J., BEDNARIK R. Gaze–grabber distance in expert and novice forest machine operators: the effects of automatic boom control. In: *ACM Symposium on Eye Tracking Research and Applications (ETRA '20 Adjunct)*, Stuttgart and Germany. Association for Computing Machinery (ACM), 2020, pp. 1–7, doi: 10.1145/3379157.3391414.

[17] CIENFUEGOS M., MAYCOCK J., NACERI A., DÜSTERHUS T., KÕIVA R., SCHACK T., RITTER H. Exploring motor skill acquisition in bimanual coordination: insights from navigating a novel maze task. *Scientific Reports*. 2024, 14(1), pp. 18887, doi: 10.1038/s41598-024-69200-1.

[18] SHISHOV N., MELZER I., BAR-HAIM S. Parameters and Measures in Assessment of Motor Learning in Neurorehabilitation; A Systematic Review of the Literature. *Frontiers in Human Neuroscience*. 2017, 11, pp. 82, doi: 10.3389/fnhum.2017.00082.

[19] YEGANEH DOOST M., ORBAN DE XIVRY J.-J., BIHIN B., VANDERMEEREN Y. Two Processes in Early Bimanual Motor Skill Learning. *Frontiers in Human Neuroscience*. 2017, 11, pp. 618, doi: 10.3389/fnhum.2017.00618.